IAC–16–C1.4.1x35306

STATISTICAL MULTICRITERIA EVALUATION OF ASTEROID DEFLECTION METHODS

Nicolas Thiry
University of Strathclyde, United Kingdom, nicolas.thiry@strath.ac.uk

Massimiliano Vasile
University of Strathclyde, United Kingdom, massimiliano.vasile@strath.ac.uk

We assess in this paper 3 different deflection approaches for a wide range of virtual collision scenarios: the kinetic impactor is considered for the family of impulsive deflection methods whereas the family of slow-push methods is represented by the laser ablation and the ion beam shepherd techniques. A sample of 100 deflection scenarios was created from realistic distribution of PHA eccentricities, semi-major axis and inclination and, for each case, a virtual impactor scenario was formed by modifying the argument of perigee so that the virtual PHA crosses the ecliptic plane at a distance of 1AU. A fixed asteroid mass of 4×10^9 kg and 10^{10} kg were both considered in this study, corresponding to an estimated diameter of 156m and 212m respectively. A realistic model of each deflection method was integrated within a systematic approach to size the spacecraft and predict the achievable deflection for a given mission. The available mass to perform the deflection depends on the transfer strategy. For the case of the kinetic impactor, a direct injection using a multiple-revolution Lambert arc is considered. For the case of slow-push methods, a low-thrust transfer is retained in order to take advantage of the large electrical power available which would otherwise remain unused during the transfer phase. In all cases, the launch capability of Delta 4 Heavy RS-68A upgrade version (10-tons at $c_3 = 0$) is assumed. Finally, global optimization techniques are used to compare the methods with respect to 2 criteria: the minimum duration between the departure date and the time of virtual impact required to deflect the PHA by more than 2 Earth radii or the miss-distance achieved within a total duration of 10 years. Our results provide an interesting insight into the range of applicability of individual deflection methods and suggest the need to develop multiple methods in parallel for a global mitigation of possible threats.

I. Introduction

Near Earth Asteroids (NEAs) are arbitrarily defined as asteroids with perihelia less than 1.3 astronomical units (AU). Potentially hazardous asteroids (PHAs) represent a portion the NEAs whose current orbits can approach the Earth's orbit to within 0.05 AU. Thus, in terms of their origin and physical nature, PHAs are not different from other NEAs but they just happen to come close enough to Earth at the present time so that close planetary encounters could conceivably perturb their orbits so as to permit an actual near-term collision, hence they warrant careful tracking(Chapman (2004)).

Several mitigation methods have been proposed over the years to deflect the trajectory of a potentially hazardous asteroid (PHA) from a collision course with the Earth. Most of the strategies proposed fall into 2 categories: impulsive and slow-push. Impulsive strategies are usually modeled with an instantaneous change of momentum given by, for example,

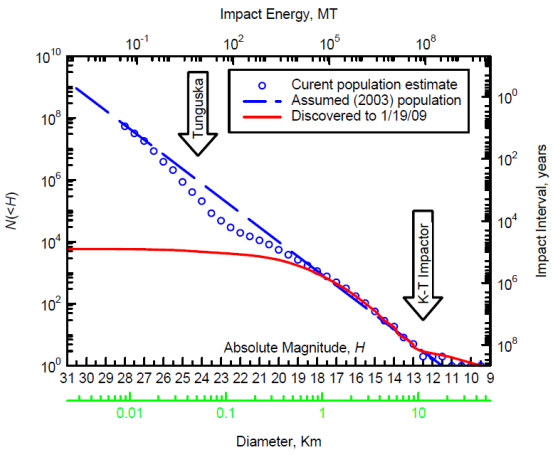

Fig. 1: The cumulative population of asteroid and their impact frequency on the Earth from Harris and DAbramo (2015)

a nuclear explosion (nuclear interceptor) or the hypervelocity impact of a spacecraft (kinetic impactor) with the asteroid. Slow-push methods, on the other hand, allow for a more controllable deflection maneuver by exerting a small continuous and controllable force on the asteroid over an extended period of time. We compare in this paper 3 different deflection approaches for a wide range of collision scenarios: the kinetic impactor is considered for the family of impulsive methods whereas the family of slow-push methods is represented by the laser ablation and the ion beam shepherd techniques. A sample of 100 deflection scenarios were created from realistic distribution of PHA eccentricities, semi-major axis and inclination. In all cases, a virtual impactor scenario was formed by modifying the argument of perigee so that the virtual PHA crosses the ecliptic plane at a distance of 1AU. A fixed asteroid mass of 4×10^9 kg and a larger mass of 10^{10} kg are considered in this study, corresponding to an estimated diameter of 156m and 212m respectively. In particular, the first choice corresponds the size of asteroid 2011AG5 which was previously considered by NEOSHIELD while the second choice approaches the limit of our current detection rate, if one refers to the plot of Harris and DAbramo (2015) on Fig.1. We integrated a realistic model of each deflection method within a systematic approach to size the spacecraft and predict the achievable deflection for a given mission epoch. The available mass to perform the deflection depends on the transfer strategy. For the case of the kinetic impactor, a direct injection using a multiple-revolution Lambert arc is considered. For the case of slow-push methods, a low-thrust transfer is retained in order to take advantage of the large electrical power available which would otherwise remain unused during the transfer phase. In all cases, the methods consider the use of an identical interplanetary launch capability (10-tons at $c_3 = 0$), equivalent to that of Delta 4 Heavy RS-68A upgrade version. Global optimization techniques are finally used to compare the methods with respect to 2 criteria: the minimum duration between the departure date and the time of virtual impact required to deflect the PHA by more than 2 Earth radii or the miss-distance achieved within a maximum duration of 10 years.

II. Asteroid Sampling Strategy

II.i PHA Distribution

As in the work of Bach, the undeflected motion of the PHAs considered in this work is approximated by Keplerian orbits in a heliocentric frame and the Earth orbit is approximated with an exact circle of radius 1AU. Intuitively, this simplification induces two necessary but not sufficient conditions on the semi-major axis a and eccentricity e for impacting PHAs:

$$a(1-e) < 1\text{AU} \text{ and } a(1+e) > 1\text{AU} \qquad [1]$$

Using the criterion of Eq.1, we retrieved 8273 PHAs from the NEODyS database presently maintained at the University of Pisa*. The distribution of these PHAs can be seen on Fig.2 where the green lines represent the necessary crossing condition of Eq.1.

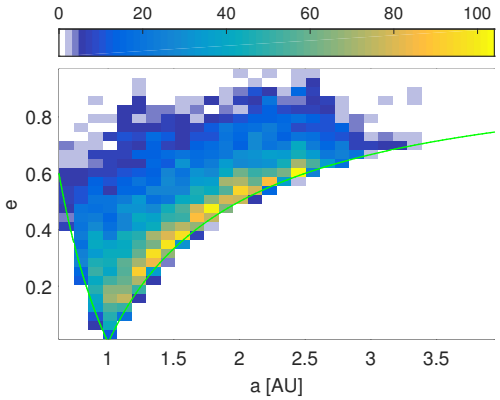

Fig. 2: Distribution in semi-major axis and eccentricity of all known PHAs with an orbit crossing a Sun-centered sphere with radius 1AU

II.ii Virtual Impactor Model

Fixing the semi-major axis, eccentricity and inclination with their actual value from the extracted database, one independent element remaining to fix is the longitude of the ascending node node Ω of the PHA's orbital plane with respect to the ecliptic. However, since we neglect the small minute Earth orbit eccentricity, the impact epoch is arbitrary and we can choose to fix $\Omega = 0$ so that the PHA's orbital planes crosses the ecliptic along the vernal equinox direction. The last parameters to fix are the argument of perihelion ω and the true anomaly θ of the PHA at the impact epoch t_{MOID}. From the above simplifications, the argument of perihelion and the true anomaly may only adopt two distinct values to respect the impact condition:

$$1\text{AU} = \frac{a(1-e^2)}{1+e\cos\omega} \text{ and } \theta = 2\pi - \omega \qquad [2]$$

*http://newton.dm.unipi.it/neodys/

The two solutions of Eq.2 correspond to an impact with the ascending or the descending branch of the PHA respectively.

II.iii Sampling Strategy

We formed a sample of virtual impactors by randomly selecting 100 PHAs in the NEODyS database, using the method described in sec.2.2 and considering an equal probability of impact with the ascending or the descending branch of the PHAs. The distributions in semi-major axis, eccentricity and inclination of this test sample are plotted for further reference in Fig.3.

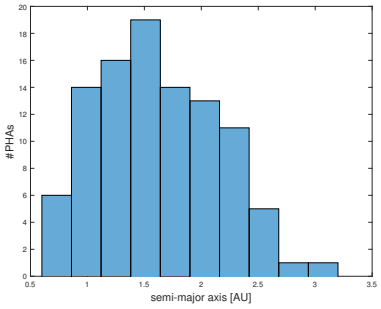

(a) semi-major axis

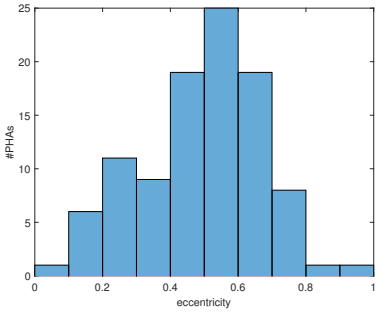

(b) eccentricity

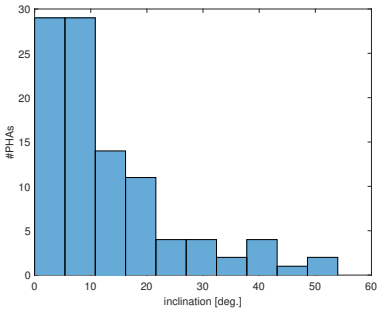

(c) inclination

Fig. 3: Distribution of the 100 PHAs randomly sampled from the NEODyS database

III. Deflection Methods

III.i Kinetic Impactor

The idea of the kinetic impactor is to impart a slight alteration in the trajectory of an asteroid by colliding a spacecraft into it at high velocity. We assume for this method a direct injection into a transfer orbit consisting in a multi-revolution Lambert arc. Therefore the mass $m_{s/c}$ of the spacecraft and its relative velocity $\delta v_{s/c}$ at the deflection date t_d are a function of both the time of flight ToF and departure date t_D for the mission as well as the interplanetary injection capability of the launcher considered. Fig. 4 shows the launch capability of the Delta 4 Heavy RS-68A upgrade version considered throughout this study as a function of the C_3 escape energy [km^2/s^2].

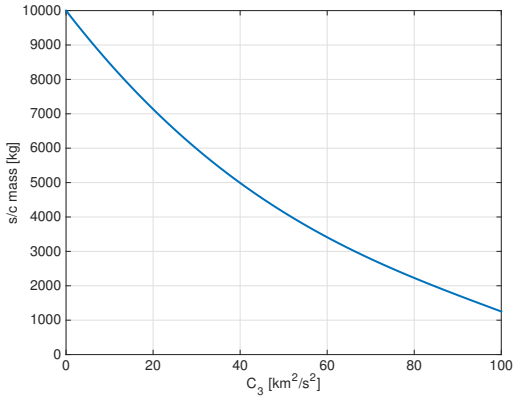

Fig. 4: spacecraft mass $m_{s/c}$ as a function of the C_3 escape energy from the regression laws of Wise et al. (2010) for the Delta IV Heavy RS-68A upgrade version

Having computed those for a given trajectory, the variation of velocity imparted by the spacecraft to the asteroid is computed by the angular momentum conservation equation, considering a momentum enhancement factor $\beta = 1$:

$$\delta v = \beta \frac{m_{s/c}}{m_{AST}} \delta v_{s/c}\,, \qquad [3]$$

The modified orbit can be computed from the instantaneous change in the asteroid velocity vector $\delta \mathbf{v} = (\delta v_t, \delta v_n, \delta v_h)$ along the tangential, normal and

out-of plane directions:

$$\begin{aligned}
\delta a &= \frac{2a^2V}{\mu}\delta v_t\,, \\
\delta e &= \frac{1}{V}\Big[2(e+\cos\theta_d)\delta v_t - \frac{r}{a}\sin\theta_d\delta v_h\Big]\,, \\
\delta I &= \frac{r\cos\varpi_d}{h}\delta v_h\,, \\
\delta\Omega &= \frac{r\sin\varpi_d}{h\sin I}\delta v_h\,, \\
\delta\omega &= \frac{1}{eV}\Big[2\sin\theta_d\delta v_t + \Big(2e+\frac{r}{a}\cos\theta_d\Big)\delta v_n\Big] \\
&- \frac{r\sin\varpi_d\cos I}{h\sin I}\delta v_h\,, \\
\delta M_d &= -\frac{b}{eaV}\Big[2\Big(1+\frac{e^2r}{p}\Big)\sin\theta_d\delta v_t + \frac{r}{a}\cos\theta_d\delta v_n\Big]\,,
\end{aligned} \qquad [4]$$

where θ_d, M_d are the true and mean anomaly at the deflection epoch, $\varpi_d = \theta_d + \omega$ is the true longitude, $p = a(1-e^2)$ is the semilatus rectum, $h = \sqrt{\mu a(1-e^2)}$ is the angular momentum, $r = p/(1+e\cos\theta)$ is the orbital radius, and V is the instantaneous asteroid velocity modulus. The achieved deviation $\delta\mathbf{r}$ can be computed from the variation of the orbital parameters

$$\delta\mathbf{k} = [\delta a,\, \delta e,\, \delta I,\, \delta\Omega,\, \delta\omega,\, \delta M]$$

by propagating the modified orbit and computing the Cartesian distance between the Earth and the NEO at the time of expected minimum orbit interception distance (t_{MOID}). From the deflection $\delta\mathbf{r}$ the impact parameter b at the time of the MOID can be computed (see Fig.5a where $\mathbf{V}_{NEO}$ is the velocity of the deviated asteroid with respect to the Earth). The impact plane can be defined as the plane centered in the Earth and perpendicular to the velocity vector of the undeviated asteroid with respect to the Earth, $\mathbf{U}_{NEO}$, at the time of the impact (see Fig.5b where $\mathbf{v}_E$ is the velocity of the Earth). The deflection vector $\mathbf{x}_b$ in the b-plane coordinates can be expressed as:

$$\mathbf{x}_b = [\xi\ \ \eta\ \ \zeta]^T = \left[\widehat{\xi}\ \ \widehat{\eta}\ \ \widehat{\zeta}\right]^T \delta\mathbf{r} \qquad [5]$$

where:

$$\widehat{\eta} = \frac{\mathbf{U}_{NEO}}{U_{NEO}}, \quad \hat{\xi} = \frac{\mathbf{v}_E \wedge \widehat{\eta}}{\|\mathbf{v}_E \wedge \widehat{\eta}\|}, \quad \hat{\zeta} = \widehat{\xi} \wedge \widehat{\eta} \qquad [6]$$

The impact parameter b is then defined as (Milani and Valsecchi (1999)):

$$b = \sqrt{\xi^2 + \zeta^2} \qquad [7]$$

and provides an accurate estimation of the miss-distance. Fig.6 shows the achieved impact parameter as a function of departure date and time of flight considering a kinetic impactor injected into a transfer orbit by a Delta 4 Heavy rocket to 2011AG5.

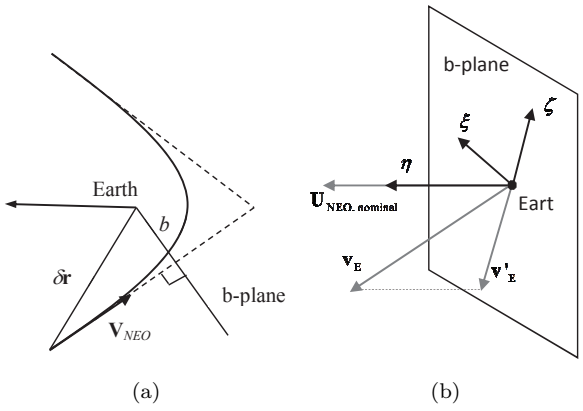

Fig. 5: The b-plane and the impact parameter b

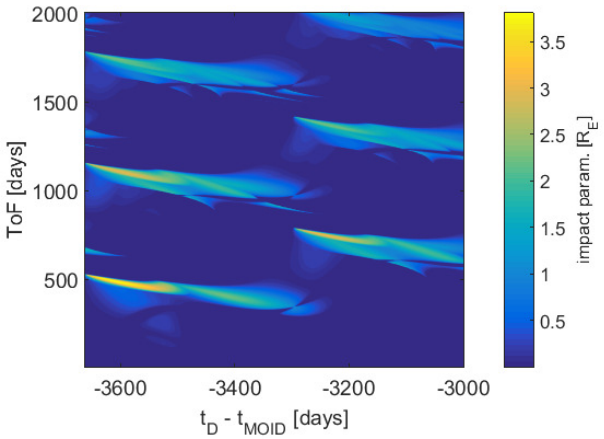

Fig. 6: impact parameter as a function of the departure date t_D and time of flight ToF for 2011AG5

III.ii Ion Beam Shepherd

The IBS method considers the use of an Isp-efficient Ion Engine to impart a small push on the asteroid over an extended duration of operation. In order to maintain its position at a vantage point, engines need to be positioned on both sides of the spacecraft to balance the thrust coming from the engine propelling the ions on the PHA. A low-thrust transfer is considered in the case of this method, which allows using the electric propulsion system also during the transfer phase. The spherical shaping method intro-

duced in the work of Novak and Vasile (2011) was used to compute low-cost low-thrust trajectories as a function of the ToF and departure epoch for the the mission. An example of calculated trajectory to asteroid 2011AG5, requiring a Δv of 7.8km/s is shown on Fig.7.

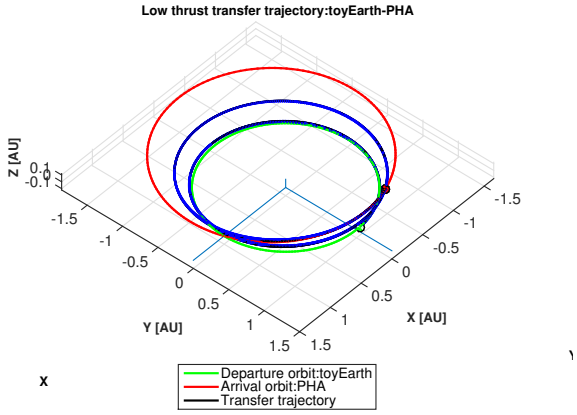

(a)

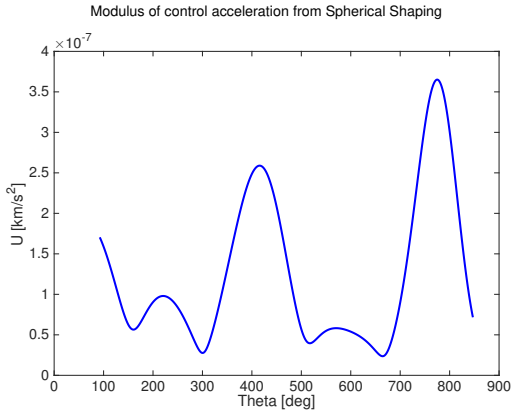

(b)

Fig. 7: Example of calculated low thrust transfer trajectory and Modulus of the control acceleration with the Spherical Shaping method for ToF = 847days and $t_D = -3615$ days before virtual impact with 2011AG5

Considering an Isp of 3000 s and given a departure mass, our algorithm returns the mass at arrival but also the maximum thrust and power required to realize this transfer. From this information, the mass required for the EPS, power systems and radiators can be computed, assuming Solar Electric Propulsion as a primary power source (SEP) and an oversizing coefficient that can vary between 1 and 10. Oversizing allows to increase the thrust that can be generated during the later deflection phase but also penalizes the amount of propellant mass that will be available during the deflection phase.

Efficient (30% from solar to electrical power) triple junction solar arrays are considered in our study. In line with the predicted performance of Orbital ATK's UltraFlex and Megaflex arrays, we consider a specific array mass of 10kg/kW throughout this study, scaling with the power required at 1AU. An additional 5kg/kW, scaling with the peak power at perihelion, models the other components of the power subsystem, including PCDU.

Typically, the Electric Propulsion Subsystem (EPS) comprises three core elements:

- The thruster assembly which includes in this case the thrusters and the gimbals on which they can be mounted to control the thrust orientation. A specific mass of 2kg/kW together with a thrust to power ratio of 46mN/kW are considered in the calculations and the thrusters are sized with respect to the peak thrust delivered during mission.
- The Power Processing Unit (PPU/TSU) which supplies the high voltage current required for the ion engines to work efficiently. The Thruster Selection Unit (TSU) itself allows to select the thruster fed by the PPU. The PPU/TSU is assumed to scale with the peak power during the mission with a specific mass amounting to 6kg/kW.
- The Xenon Feed System (XFS) or Flow Control Unit (FCU) which usually includes a high pressure tank, a Xenon Control Assembly (XCA) which regulates the pressure and Xenon flow rate to the thrusters and the plenum tanks. The mass of the XFS is assumed to scale with the peak thrust with a specific mass of 1kg/kW, which excludes the Xenon tank which itself is assumed to scale linearly with the propellant mass. The Dawn Xenon tank had a volume of 269L, could store up to 425kgs of Xenon and had a mass of 21.6kgs, giving a tankage fraction of 5%.

A parametric mass model was also considered for the other subsystems, including harness (5% of the wet mass), structure (20% of the dry mass), AOCS (5% of the wet mass), as well as a non-scalable mass of 50kg to telecommunications and data handling. Radiators are also scaled with respect to the maximum available power, considering a heat sink of 50% of the available power, ability of the radiator to re-radiate 400W per square meter and an areal density

of 5kg/m^2. Eventually, any remaining mass is allocated to the additional propellant that will be used during the deflection phase (minus the mass required to increase the size of the tanks and structure). If no mass is left prior to that step, the mission is considered unfeasible with that particular combination of departure date, time of flight and oversizing coefficient. Considering a wet mass of 1000 kg, the transfer of Fig.7, as well as an oversizing factor of 1, Fig.8 illustrates the resulting mass budget. The IBS spacecraft for this particular scenario would be able to generate a nominal thrust (in deflection mode) of 110mN and nominal input power level of 4.78kW at a distance of 1AU from the Sun.

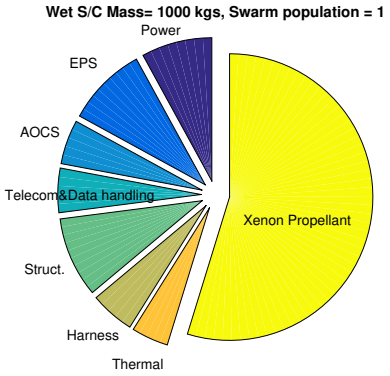

Fig. 8: IBS mass budget for ToF = 847days and $t_D = -3615$ days before virtual impact with 2011AG5 and an oversizing factor of 1

The deflection phase starts as soon as the spacecraft has rendezvoused with the PHA. During that phase, it is assumed that the engines work at the maximum of their capability given the available power generated by the solar arrays at the current distance from the sun. Only half of the thrust can be used for the deflection as the other half is needed for station-keeping of the IBS. The acceleration on the asteroid is assumed to be also imparted in the tangential direction in average and is computed by

$$u_t = \frac{F_{\rm IBS}}{m_{\rm AST}} \qquad [8]$$

The deflected orbit is then calculated by integrating Gauss' planetary equations from the time when the t_d deflection starts until the time of the virtual impact $t_{\rm MOID}$. If, at some point during the deflection, the amount of propellant available has been consumed, a null acceleration is considered for the remaining part of the integration.

$$\begin{aligned}
\frac{da}{dt} &= \frac{2a^2V}{\mu}u_t\,,\\
\frac{de}{dt} &= \frac{1}{V}\Big[2(e+\cos\theta)u_t - \frac{r}{a}\sin\theta u_h\Big]\,,\\
\frac{dI}{dt} &= \frac{r\cos\varpi_d}{h}u_h\,, \qquad [9]\\
\frac{d\Omega}{dt} &= \frac{r\sin\varpi_d}{h\sin I}u_h\,,\\
\frac{d\omega}{dt} &= \frac{1}{eV}\Big[2\sin\theta u_t + \Big(2e+\frac{r}{a}\cos\theta\Big)u_n\Big]\\
&- \frac{r\sin\varpi_d\cos I}{h\sin I}u_h\,,\\
\frac{dM}{dt} &= -\frac{b}{eaV}\Big[2\Big(1+\frac{e^2r}{p}\Big)\sin\theta u_t + \frac{r}{a}\cos\theta u_n\Big]\,.
\end{aligned}$$

Once the deflected orbit has been computed, the miss-distance can be estimated by projecting the deflection distance on the b-plane, as explained in sec.3.1.

III.iii Laser Ablation

The laser ablation deflection method aims at exploiting the material the asteroid is made of in order to generate the required thrust. The ablated material forms a plume of vaporized material which, due to the action/reaction principle, creates a controllable and continuous thrust on the asteroid.

With the power depending on efficient (30% from solar to electrical power) triple junction solar arrays, the level of thrust is again modulated by the square of the distance to the sun during the deflection phase, which is assumed to start as soon as the spacecraft arrives to the asteroid. The conversion from input power to ablative thrust F_{abl} on the asteroid is computed through the formula

$$F_{\rm LS} = \eta_{LS} C_m P_{in}\,. \qquad [10]$$

In which η_{LS} is the electrical to optical (E/O) conversion efficiency of the laser system and C_m, the thrust coupling coefficient, which is known to vary between 10 to 100$\mu N/W_{optical}$ for most materials Phipps (2011). E/O efficiencies >39% have already been demonstrated by multi-kW spectrally beam combined fiber-coupled diode lasers (Honea et al. (2013)). Focused development under the DARPA SHEDs program has also lead to extremely high power conversion efficiency in the 9xx-nm wavelength band, leading to diode bars with efficiency in excess of 74% and a clear route to efficiencies superior to 85%

at room temperature (Crump et al. (2007)). With demonstrated slope efficiency of optical fibers on the order of 80% (Jeong et al. (2004)) and a demonstrated efficiency of spectral beam combining techniques of 91% (Drachenberg et al. (2011)), we consider in this paper a global E/O efficiency of 50%.

Detailed calculations performed on Forsterite by Thiry et al. (2016) indicate that the coupling coefficient of a CW laser operating under the plasma formation intensity near the 1 micron wavelength is dictated mainly by 2 parameters: the laser intensity Φ[W/m^2] which depends on the laser output power and focusing ability of the optics as well as the mean time available to heat the material which is roughly proportional to the ratio between the laser beam diameter and the relative speed of the asteroid surface with respect to the laser beam (on the order of 8cm/s if one considers the spin-limit of a 212m asteroid). Fig.9 shows the result of these calculation for Forsterite, a main constituent of S-type asteroids which are thought to dominate the population in the inner belt. For typical mean heating times on the order of 10-100ms and typical CW laser beam intensities on the order of 1GW/m^2 envisioned in our laser system, one can see from this chart that the thrust coupling has a value around 55-60$\mu N/W$ and will only be weakly affected by the temporal changes in operating conditions due to the variation of input power with respect to the square distance to the sun. To generate the intensity levels required, the optics should be designed using the diffraction limit focusing capability at the shooting distance. The optical components should also be designed so that they are exposed to intensity levels well under their damage threshold. As an example, an optics with a primary mirror of 60cm diameter would be enough to generate a 3mm laser spot at a 1km shooting distance. For a 10kW laser, this would correspond to an intensity of 1.4GW/m^2 at the focal spot, but only 35kW/m^2 on the primary mirror.

Plasma effects are also not expected to play any role under CW laser irradiation below intensity levels of 10GW/m^2, which are required to accelerate the free electrons in the vapor by inverse Bremsstrahlung until their kinetic energy becomes sufficient to ionize the atoms of the vapor by an avalanche process, according to Poueyo-Verwaerde et al. (1993). A model to predict the thrust coupling coefficient in the Plasma regime has been developped by Phipps et al. (1988) for pulsed laser systems and it is interesting to compare the peak coupling predicted by this model with the values predicted by our CW model.

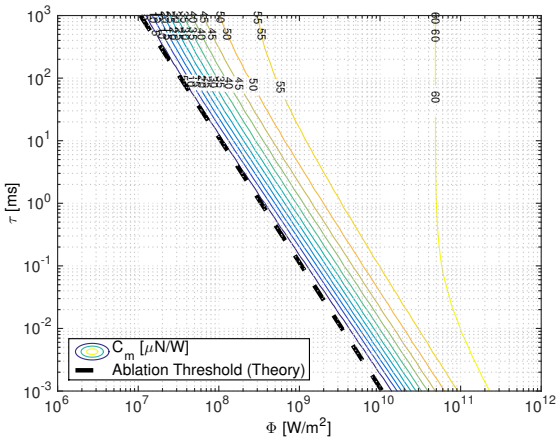

Fig. 9: Thrust coupling coefficient C_m as a function of the mean heating time τ and beam power density Φ for a CW laser.

In this model, the plasma coupling C_{mp} coefficient was empirically found to follow a power law:

$$C_{mp}(\mu N/W) \approx 184 \frac{\Psi^{9/16}}{A^{1/8}\left(\Phi\lambda\sqrt{\tau}\right)^{1/4}} \qquad [11]$$

in which τ is the pulse duration, λ the laser wavelength and Ψ depends on the average atomic number A and the average ionization state Z as:

$$\Psi = \frac{A}{2\left(Z^2(Z+1)\right)^{1/3}} \qquad [12]$$

Phipps et al. (1988) noted that the optimal coupling happens for values of intensity and pulse duration such that $\Phi\sqrt{\tau}$ = 8.5E+08W s$^{1/2}$/m^2, which is about twice the value at which plasma ignition occurs for pulses <1ms. Initially, ionization enhances the thrust coupling coefficient because, despite requiring more energy to ionize the plume, increased absorption by the plume increases the thermal coupling coefficient(Rosen et al. (1982)). Using the same estimation as Phipps (2014), we assumed a single stage ionization (Z=1) and injected the relevant values in Eq.11 to compute the optimal thrust coupling coefficient for a wide range of atoms and materials encountered in asteroid for a 1μm laser wavelength. Our results are summarized in Table 1. Interestingly, the value predicted is about 25% higher than our own calculation, which neglected plasma effects. In the rest of this paper, we will consider a conservative value of 40$\mu N/W$, accounting also for possible loss due to the shape irregularity of the asteroid and the fact

Symbol	Mg	Fe	Si	O	C	Mg2SiO4	Fe2SiO4
Name	Magnesium	Iron	Silicon	Oxygen	Carbon	Forsterite	Fayalite
A	24	26	28	16	12	-	-
$C_{mp}^{opt}(\mu N/W)$	80	83	86	67	59	75(avg.)	79(avg.)

Table 1: Optimal thrust coupling predicted by Eq.11 for various materials encountered in asteroids

that the laser ablation thrust can only be oriented in the desired direction tangential with respect to the PHA trajectory in average. In fact, as explained by Vetrisano et al. (2015, 2016) a smart laser steering strategy would allow to improve further the thrust directional efficiency.

As in the case of the IBS method, a low-thrust transfer is assumed for this method, which allows using the large power available (the laser is only used once the spacecraft has rendezvoused with the asteroid) to be used by an electric propulsion system during the transfer phase. Initially, the preliminary sizing of the different subsystems is parametrized in the same way as with the IBS method (without oversizing coefficient). Some of the remaining dry mass available is then allocated to the laser system in order to match with the available power or, if no mass was left at this point, this particular mission is considered non-feasible. It is assumed that the laser system (including optics) scales with the peak power with a specific mass of 15kg/kW (current fibre-coupled diode laser are already available with a specific mass of 1kg/kW for welding applications). If there is still mass left after this step, the size of the power system, laser system and radiators is increased until all the mass has been allocated. Considering the same scenario as for the IBS, a summary of the mass budget considering a wet mass of 1000kg is given in Figure 10. For this specific case, the laser system would deliver an estimated nominal ablative thrust of 168mN and nominal input power level of 8.4kW at a distance of 1AU from the Sun. For comparison, Nasa's Dawn spacecraft, which recently visited the dwarf planet Ceres using 3 NSTAR gridded ion-thrusters and achieved a record cumulated Δv of 14km/s, had a wet mass of 1240 kg with 425 kg of Xenon propellant, a dry spacecraft mass of 815 kg and a solar array of 36.4m^2 able to deliver 10.3kW at 1AU. Finally, the deflection is computed as in the case of the IBS, except that the acceleration is imparted for the whole duration until impact epoch.

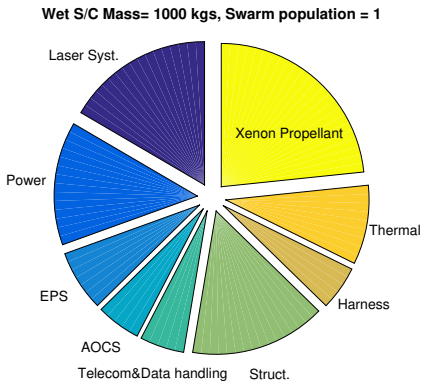

Fig. 10: LS mass budget for ToF = 847days and $t_D = -3615$ days before virtual impact with 2011AG5

Contamination Considerations

According to previous studies(Gibbings et al. (2013)), the impingement with the plume of gas and debris, generated by the ablation process, could build up enough material on the surface of the solar arrays to reduce the output power below the ablation threshold. At the same time it was shown that this contamination has a limited impact on the laser itself and related optics. Furthermore, as shown in the ESA LightTouch2 study (Vasile et al. (2013)), by properly positioning the spacecraft with respect to the asteroid, aligning the arrays with the plume and adding whipple shields the effect of contamination can be mitigated to the point that they can be considered negligible over the lifetime considered in this paper.

IV. Optimisation Procedures

The optimisation of the deflection strategies requires the global exploration of the parameter space. Furthermore, it is desirable to investigate the trade-off between warning time and achievable miss distance. For this reason we used two global optimisation procedures one for single objective and the other for multi-objective optimisation of multi-modal functions: MPAIDEA(Di Carlo et al. (2015)) and

MACS2(Ricciardi and Vasile (2015)). In the following we briefly present how each optimisation approach works and how it was used in the context of this paper.

IV.i Optimisation with MPAIDEA

For all methods, the impact parameter can be computed as a strongly non-linear function of the the departure date t_D and the time of flight ToF, but also the oversizing coefficient in the case of the IBS method. For each mission scenario we globally explore the space of possible departure dates, transfer times and oversizing coefficients (in the case of the IBS) with a memetic algorithm called multi-population adaptive inflationary differential evolution algorithm (MP-AIDEA).

MP-AIDEA is a multi-population adaptive version of Inflationary Differential Evolution. Inflationary Differential Evolution is based on a simple but theoretically rigorous re-start rule that allows an effective evolutionary heuristic, like DE, to avoid stagnation. MP-AIDEA extends this concept by automatically adapting some key parameters governing the convergence of the algorithm. At every restart of the evolutionary process a local search is run from the best individual in the population of candidate solutions. All the local minima are then stored in an archive. The restart process is such that the population is initialised outside a trust region enclosing clusters of minima stored in the archive. MP-AIDEA has been extensively tested on a range of difficult problems including real-world applications(Di Carlo et al. (2015)).

The decision variables time of flight, ToF, and mission duration, $t_{\text{mission}} = t_{\text{MOID}} - t_D$, are are limited by box constrains. The relevant parameters used during the global optimisation process can be found in Table 2

Method	ToF(sid. days)	t_{mission}(sid. days)	#agents	#pop.	#Fevals
KI	[0,1000]	[1000,3662.42]	10	4	10000
IBS	[300,2000]	[2000,3662.42]	15	4	1200
LA	[300,2000]	[2000,3662.42]	10	4	1000

Table 2: Parameters and box constrains used during the optimisation with MP-AIDEA

During each function evaluation, we also run an internal loop to evaluate the solution within the feasible range of number of revolutions for the trajectory computed by the Lambert solver and the spherical shaping algorithm. When more than one transfer are feasible for the combination of ToF and t_D, our fitness function only returns the solution with the number of revolution that provides the best miss-distance.

IV.ii Optimisation with MACS2

Multi-Agent Collaborative Search (MACS2) is a memetic multi-objective optimisation framework in which a population of virtual agents implement a number of local search heuristics intermingled by global communication heuristics that help the population to reconstruct an approximation of the Pareto set. Each agent explores a neighborhood of the parameter space, stores Pareto optimal solutions in an archive and shares information with the other agents in the population. For more specific information please refer to Ricciardi and Vasile (2015).

MACS2 was used to optimize both the departure date and the impact parameter. To this end, the biobjective fitness function can be formulated in term of the impact parameter and mission duration. The decision variables were also reformulated with box constrains on the time of flight ToF and deflection duration $t_{\text{defl}} = t_{\text{MOID}} - t_d$, with $\text{obj}_2 = \text{ToF} + t_{\text{defl}}$.

The relevant parameters used during the global optimisation process can be reviewed in Table 3

Method	ToF(sid. days)	t_{defl}(sid. days)	#agents	#Fevals
KI	[0,1000]	[0,3662.42]	150	14000
IBS	[300,2000]	[0,3662.42]	150	3000
LA	[300,2000]	[0,3662.42]	150	3000

Table 3: Parameters and box constrains used during the optimisation with MACS2

IV.iii Example with (99942) Apophis (scaled down to 10^{10}kg) and 2011AG5 (4×10^{9}kg)

As an example of multi-objective optimization, we show here the pareto fronts we obtained by considering the maximum miss-distance in minimizing the total duration from mission departure to the MOID epoch. The two asteroids considered in this case are a scaled down version of (99942) Apophis and the actual asteroid 2011AG5 previously considered by NEOSHIELD. The results are represented on Fig.11 for (99942) Apophis and Fig.12 for 2011AG5. Interestingly, note that the MACS2 clearly identified discrete departure windows in the case of a Kinetic Impactor method, which can be explained by the use of an impulsive transfer strategy for this method. The pareto optimum identified on Fig.12a for a duration of 10 years is remarkably consistent with the maximum value found by evaluating the miss-distance over the entire parameter space on Fig.6.

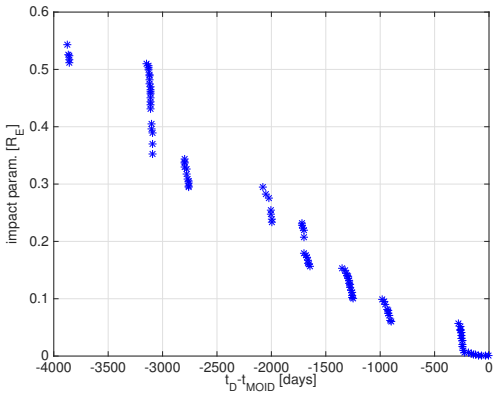

(a) Kinetic Impactor

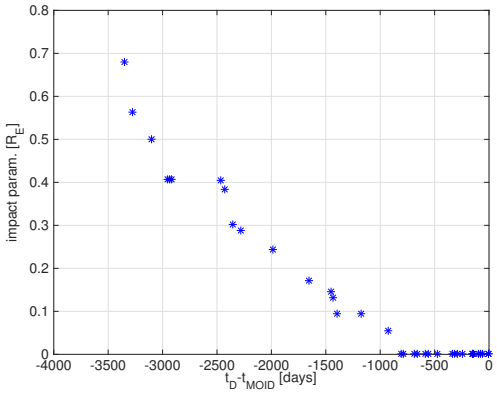

(b) Ion Beam Shepherd

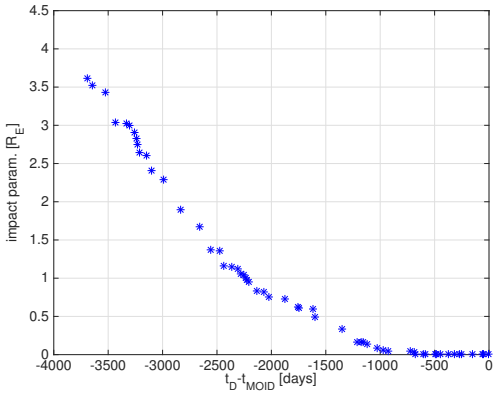

(c) Laser Ablation

Fig. 11: Maximum miss-distance and maximum departure date for the deflection of a 10^{10}kg, 212m diameter Apophis-like asteroid with a S/C launched by Delta 4 heavy

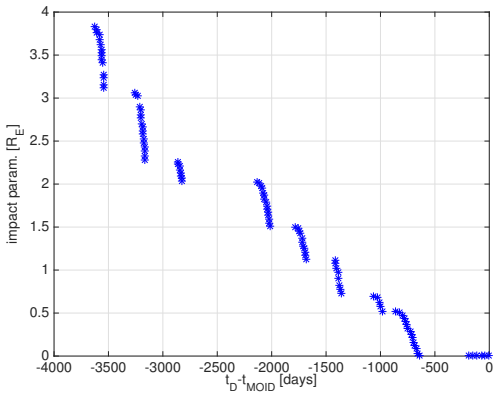

(a) Kinetic Impactor

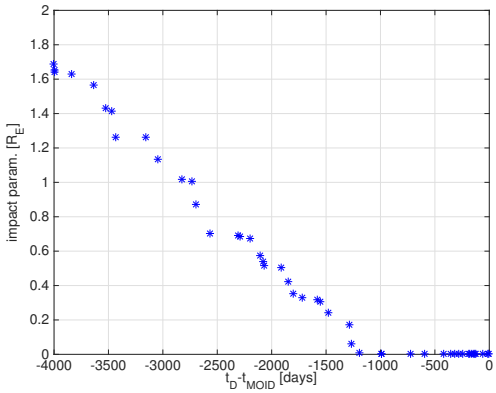

(b) Ion Beam Shepherd

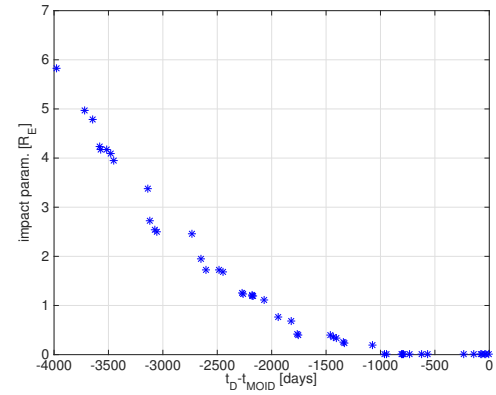

(c) Laser Ablation

Fig. 12: Maximum miss-distance and maximum departure date for the deflection of 2011AG5 (4 $\times 10^9$kg, 156m diameter) with a S/C launched by Delta 4 heavy

V. Results and Discussion

We computed the maximum miss-distance within 10 years ($t_{\text{MOID}} - t_D < 10$years) and the minimum mission time ($t_{\text{MOID}} - t_D$) to achieve a miss-distance superior to 2 Earth radii. Note that, for the latter case, we tricked our multi-objective solver into finding the minimum time required to achieve a desired impact parameter $b > 2R_E$ by reformulating the deflection fitness function as $(b - 2R_E)^2$ if $b < 2R_E$ or 0 otherwise.

The results of the maximum miss-distance obtained with MP-AIDEA can be seen on Fig.13 and Fig.14 for the case of a 212m and 156m asteroid respectively. As one could reasonably expect, the achievable miss-distance scales with mass of the asteroid. The Kinetic impactor outperformed the other methods in 78% of the scenarios. The laser ablation method had the edge in the remaining 22% of the cases, which corresponded to asteroids with easily accessible orbits from the Earth (low eccentricity, inclination and orbital period close to 1 year).

The results of the minimum time to achieve a 2 Earth radii ($2R_E$) deflection can be seen on Fig.15 and Fig.16 for the case of a 212m and 156m asteroid respectively. On these plots, red points indicate non-feasible deflection solutions within a range of 10 years between departure date and MOID epoch. 43 PHAs can be deflected by the Kinetic Impactor method, against 11 for the Laser Ablation strategy. Due to the low performances of the IBS method, we didn't include it in this second analysis. Rather, we show on Fig.15c how many targets could be deflected if either the Kinetic Impactor method or the Laser Ablation method were available. Interestingly, for the case of the 212m asteroid scenario, none of the targets deflected by the Laser Ablation method could be deflected by the Kinetic Impactor and vice-versa.

Therefore, with both options available, a total of 54 targets could be deflected at a safe distance during the close-encounter with the Earth. Somewhat similar results were obtained for the case of a 156m asteroid, although in this case the Kinetic impactor is able to deflect 84% PhAs against 46% in favor of the Laser ablation method (from Fig.13, notice that the IBS technique would still deflect as little as 2% of the PHAs in that case). Interestingly, remark again that the KI method performs badly for a subset of virtual Impactor scenario having an orbital period close to 1 year and low eccentricity for which Laser Ablation possesses a superior deflection ability. If either the Kinetic Impactor or the Laser ablation are considered, Fig.16c shows that 95% of the PHAs could be deflected.

VI. Conclusion

This paper compared a Kinetic Impactor Method, an Ion Beam Shepherd and a Laser Ablation technique for a statistically relevant set of deflection scenarios with an asteroid mass of 4 or 10×10^9kg, corresponding to a diameter of 156 and 212m respectively. It was demonstrated that the Kinetic Impactor method outperforms the other techniques in a majority of the cases. However, detailed investigation reveals that the Kinetic Impactor method performs badly for a subset of virtual Impactor scenario having an orbital period close to 1 year and low eccentricity.

For these cases, Laser Ablation demonstrated a superior deflection ability (sometimes by more than one order of magnitude), due to the existence of low-cost transfer trajectories allowing to maximize the onboard Power and Laser systems. In particular, when both the Kinetic Impactor and the Laser ablation were considered, deflection of 95% of the 156m PHAs could be achieved within a maximum duration of 10 years between departure date and MOID epoch.

Additional interest for these scenarios arises due to the fact that they represent possible targets for future exploration and exploitation missions. Therefore, our results plead for the parallel development of both technologies in the future.

Acknowledgment

The work in this paper was partially supported by the Marie Curie FP7-PEOPLE-2012-ITN Stardust, grant agreement 317185. The authors express their gratitude to Niccolò Gastaldello for implementing the Spherical Shaping algorithm used in this paper as well as Lorenzo Ricciardi and Marilena Di Carlo for their help in setting the parameters of MP-AIDEA and MACS2.

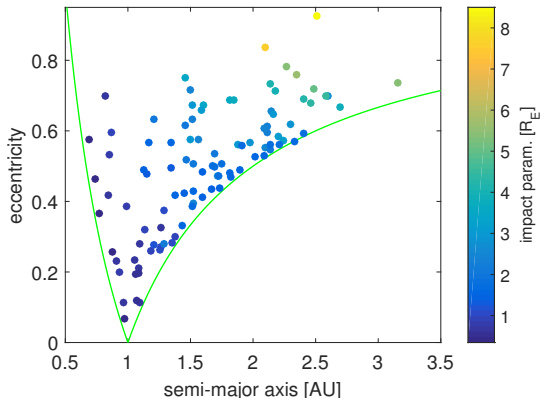

(a) Kinetic Impactor

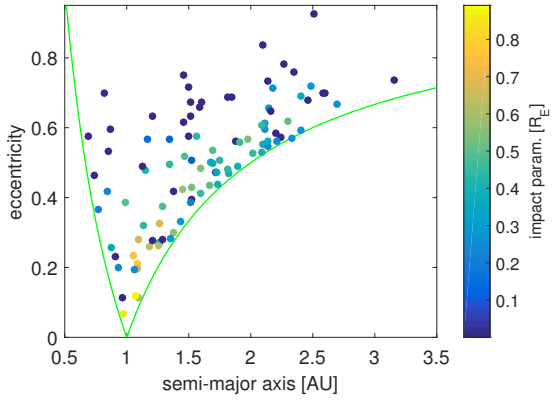

(b) Ion Beam Shepherd

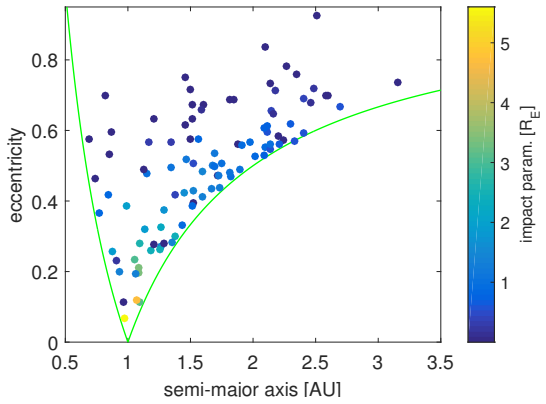

(c) Laser Ablation System

Fig. 13: Optimal deflection of a 10^{10}kg, 212m-diameter asteroid within 10 years of mission time

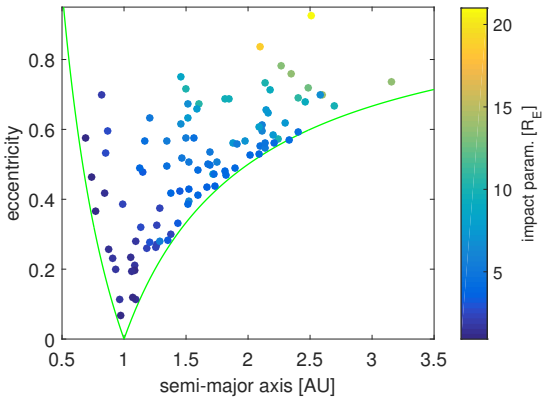

(a) Kinetic Impactor

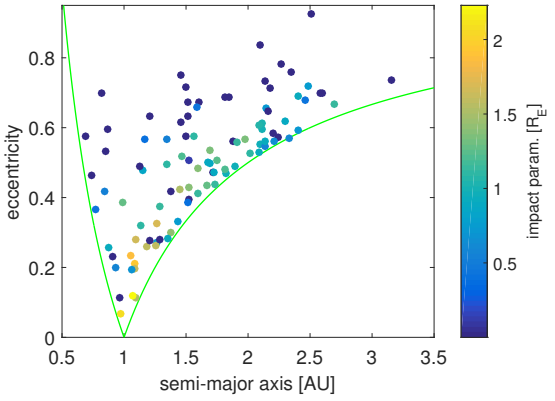

(b) Ion Beam Shepherd

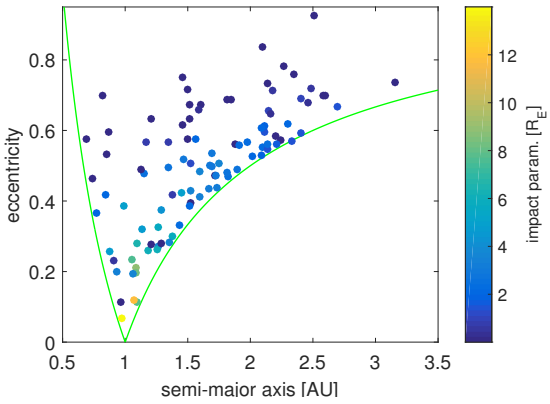

(c) Laser Ablation System

Fig. 14: Optimal deflection of a 4×10^9kg, 156m-diameter asteroid within 10 years of mission time

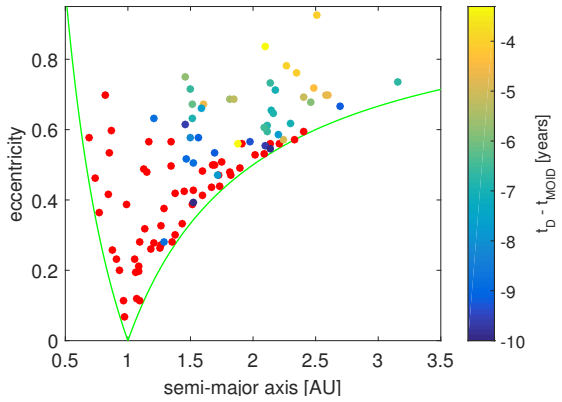

(a) Kinetic Impactor

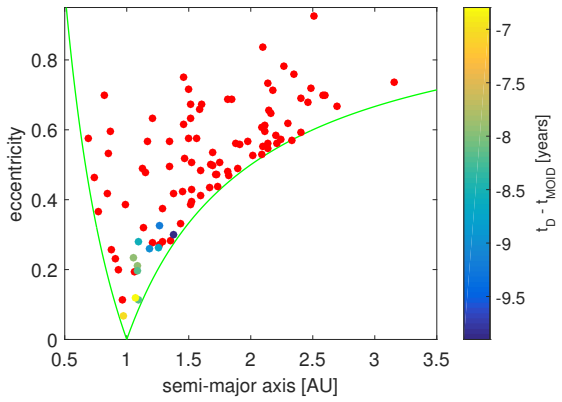

(b) Laser Ablation

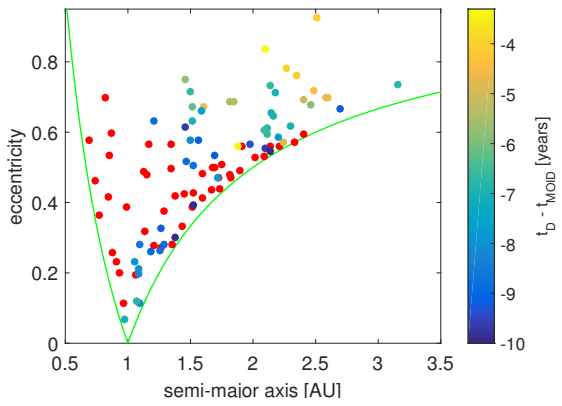

(c) Kinetic Impactor and Laser Ablation

Fig. 15: latest departure time for the deflection of a 10^{10}kg asteroid by 2 earth radii with a S/C launched by Delta 4 heavy. Red points indicate unsuccessful missions within 10 years

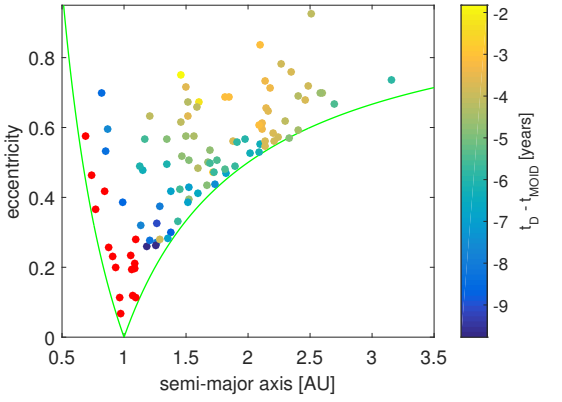

(a) Kinetic Impactor

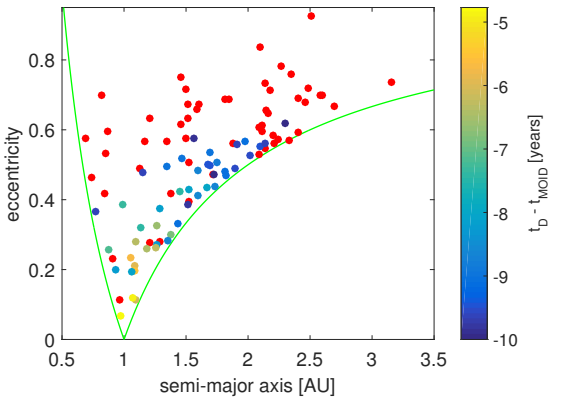

(b) Laser Ablation

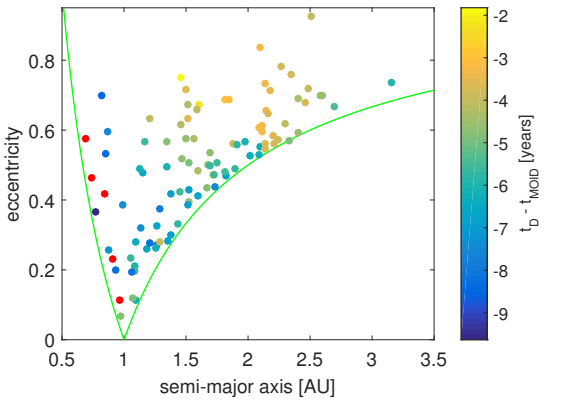

(c) Kinetic Impactor and Laser Ablation

Fig. 16: latest departure time for the deflection of a 4×10^9kg asteroid by 2 earth radii with a S/C launched by Delta 4 heavy. Red points indicate unsuccessful missions within 10 years

References

Fabian Bach. A parametric assessment of the full pha phase space, and deflection feasibility using kinetic impactors. Technical report.

Clark R Chapman. The hazard of near-earth asteroid impacts on earth. *Earth and Planetary Science Letters*, 222(1):1–15, 2004.

Paul Crump, Weimin Dong, Mike Grimshaw, Jun Wang, Steve Patterson, Damian Wise, Mark DeFranza, Sandrio Elim, Shiguo Zhang, Mike Bougher, et al. 100-w+ diode laser bars show¿ 71% power conversion from 790-nm to 1000-nm and have clear route to¿ 85%. In *Lasers and Applications in Science and Engineering*, pages 64560M–64560M. International Society for Optics and Photonics, 2007.

Marilena Di Carlo, Massimiliano Vasile, and Edmondo Minisci. Multi-population inflationary differential evolution algorithm with adaptive local restart. In *2015 IEEE Congress on Evolutionary Computation (CEC)*, pages 632–639. IEEE, 2015.

Derrek Drachenberg, Ivan Divliansky, Vadim Smirnov, George Venus, and Leonid Glebov. High-power spectral beam combining of fiber lasers with ultra high-spectral density by thermal tuning of volume bragg gratings. In *SPIE LASE*, pages 79141F–79141F. International Society for Optics and Photonics, 2011.

Alison Gibbings, Massimiliano Vasile, Ian Watson, John-Mark Hopkins, and David Burns. Experimental analysis of laser ablated plumes for asteroid deflection and exploitation. *Acta Astronautica*, 90 (1):85 – 97, 2013. ISSN 0094-5765. NEO Planetary Defense: From Threat to Action.

Alan W Harris and Germano DAbramo. The population of near-earth asteroids. *Icarus*, 257:302–312, 2015.

Eric Honea, Robert S Afzal, Matthias Savage-Leuchs, Neil Gitkind, Richard Humphreys, Jason Henrie, Khush Brar, and Don Jander. Spectrally beam combined fiber lasers for high power, efficiency, and brightness. In *SPIE LASE*, pages 860115–860115. International Society for Optics and Photonics, 2013.

Y el Jeong, JK Sahu, DN Payne, and J Nilsson. Ytterbium-doped large-core fiber laser with 1.36 kw continuous-wave output power. *Optics Express*, 12(25):6088–6092, 2004.

A. Milani and G. B. Valsecchi. The asteroid identification problem: Ii. target plane confidence boundaries. *Icarus*, 140:408–423, August 1999.

NEOSHIELD. D7.5.1: Trade offs of viable alternative mitigation concepts. Technical report.

DM Novak and Massimiliano Vasile. Improved shaping approach to the preliminary design of low-thrust trajectories. *Journal of guidance, control, and dynamics*, 34(1):128–147, 2011.

Claude Phipps. An alternate treatment of the vapor-plasma transition. *International Journal of Aerospace Innovations*, 3(1):45–50, 2011.

Claude R Phipps. L adroit–a spaceborne ultraviolet laser system for space debris clearing. *Acta Astronautica*, 104(1):243–255, 2014.

CR Phipps, TP Turner, RF Harrison, GW York, WZ Osborne, GK Anderson, XF Corlis, LC Haynes, HS Steele, KC Spicochi, et al. Impulse coupling to targets in vacuum by krf, hf, and co2 single-pulse lasers. *Journal of Applied Physics*, 64(3):1083–1096, 1988.

A Poueyo-Verwaerde, R Fabbro, G Deshors, AM De Frutos, and JM Orza. Experimental study of laser-induced plasma in welding conditions with continuous co2 laser. *Journal of applied physics*, 74 (9):5773–5780, 1993.

L. A. Ricciardi and M.o Vasile. Improved archiving and search strategies for multi agent collaborative search. In *EUROGEN*, 2015.

DI Rosen, J Mitteldorf, G Kothandaraman, AN Pirri, and ER Pugh. Coupling of pulsed 0.35-μm laser radiation to aluminum alloys. *Journal of applied Physics*, 53(4):3190–3200, 1982.

Nicolas Thiry, Massimiliano Vasile, and Emanuele Monchieri. Mission and system design for the manipulation of phos with space-borne lasers. In *2016 IEEE Aerospace Conference*, pages 1–13. IEEE, 2016.

M Vasile, A Gibbings, V Massimo, J-P Sanchez, D.G Yarnoz, S Eckersley, A Wayman, J Branco, D Burns, J-M Hopkins, C Colombo, and C McInnes. Light touch2: Effective solutions to asteroid manipulation. sysnova challenge analysis final report. Technical report, University of Strathclyde, 2013.

Massimo Vetrisano, Nicolas Thiry, and Massimiliano Vasile. Detumbling large space debris via laser ablation. In *2015 IEEE Aerospace Conference*, pages 1–10. IEEE, 2015.

Massimo Vetrisano, Juan L Cano, Nicolas Thiry, Chiara Tardioli, and Massimiliano Vasile. Optimal control of a space-borne laser system for a 100 m asteroid deflection under uncertainties. In *2016 IEEE Aerospace Conference*, pages 1–13. IEEE, 2016.

MA Wise, JM Lafleur, and JH Saleh. Regression analysis of launch vehicle payload capability for interplanetary missions. In *61st International Astronomical Congress*, 2010.